Science Advances
AAAS

advances.sciencemag.org/cgi/content/full/5/12/eaax8648/DC1

Supplementary Materials for

Extreme Zr stable isotope fractionation during magmatic fractional crystallization

Mauricio Ibañez-Mejia* and François L. H. Tissot

*Corresponding author. Email: ibanezm@rochester.edu

Published 18 December 2019, *Sci. Adv.* **5**, eaax8648 (2019)
DOI: 10.1126/sciadv.aax8648

This PDF file includes:

Monte Carlo simulations of expected $\delta^{94/90}$Zr distributions

In order to evaluate whether the observed distributions of zircon and baddeleyite $\delta^{94/90}$Zr values measured from FC-1 are in agreement with the Rayleigh fractionation model described in the main text, a series of Monte Carlo simulations were performed using Matlab®. The steps followed to perform such calculations are as follows: 1) a series of uniformly distributed random values from 0 to 1 were generated using the *rand* function; 2) these randomly generated numbers were adopted as starting values of *f* for hypothetical zircon nucleation 'seeds', and used to determine their corresponding instantaneous solid $\delta^{94/90}$Zr values using a Rayleigh fractionation model and a prescribed $\alpha_{sol\text{-}liq}$; 3) each starting nucleation 'seed' was numerically integrated using the Rayleigh fractionation model, incorporating 80% of the Zr available in its surrounding at the time of crystallization; 4) hypothetical growth-zoned seeds were used to calculate a final bulk-crystal $\delta^{94/90}$Zr value; and 5) results were re-cast into probability density functions using a Gaussian kernel and a bandwidth of 0.14 ‰. This bandwidth was determined to be optimal for calculating the kernel density estimate of our measured zircon $\delta^{94/90}$Zr distribution (see Fig. 2) using the method of (*54*), and was applied to all other kernel density estimates to facilitate direct visual comparison.

Following this approach, Rayleigh fractionation curves were calculated for the three possible fractionation coefficients discussed in the text (shown in top row of fig. S8), and synthetic probability density functions computed using $n = 10^5$ random number simulations. These expected distributions from a large number of observations are shown in the middle row of fig. S8, and clearly highlight the mismatch between the observed $\delta^{94/90}$Zr distribution and those predicted using negative values of $\Delta^{94/90}$Zr. On the other hand, the expected distribution obtained using a positive $\Delta^{94/90}\text{Zr} \approx 1.06$ (*i.e.*, preferred model discussed in the text), provides a good fit to the observed data. In order to facilitate visual comparisons between our measured results and the predicted distributions, synthetic probability density functions using $n = 42$ random number simulations (*i.e.*, same as the number of zircon crystals we analyzed here from FC-1) were also computed. The bottom row of fig. S8 shows examples of five such models for each fractionation value, which again highlights the better agreement between the measured and expected $\delta^{94/90}$Zr distributions using a positive $\Delta^{94/90}$Zr coefficient rather than a negative one.

It should be emphasized, however, that this numerical experiment is highly oversimplified and does not necessarily provide an exact representation of how our data was collected; for instance, zircon crystals treated using chemical abrasion methods prior to full dissolution do not represent complete 'integrated bulk-solids', but rather the low-radiation-damaged remnants of partially leached bulk crystals. Because there is no *a priori* expectation that $\delta^{94/90}$Zr zoning within a zircon may correlate with the extent of accumulated radiation damage, the effects introduced by chemical abrasion to the observed $\delta^{94/90}$Zr distribution are non-systematic, and thus not accurately captured by our simple numerical simulations. Nevertheless, the good general agreement between our data and calculated $\delta^{94/90}$Zr distribution using a positive $\Delta^{94/90}$Zr from this simple numerical experiment, and the clear mismatch with models calculated using negative $\Delta^{94/90}$Zr coefficients, strengthens the hypothesis that early-formed zircon from FC-1 are isotopically heavy relative to the melt from which they crystallized.

MELTS and zircon crystallization modeling

Thermodynamic simulations of equilibrium fractional crystallization of FC-1 were conducted using rhyolite-MELTS v1.2.0 (*30*, *55*), which is optimized for H_2O-bearing mafic liquids

crystallizing at moderate pressure. The major element composition of our FC-1 sample (in oxide wt.%) is SiO_2: 49.43; TiO_2: 1.38; Al_2O_3: 25.31; FeO: 4.34; MnO: 0.06; MgO: 2.11; CaO: 12.71; Na_2O: 3.24; K_2O: 0.42; P_2O_5: 0.07, determined using x-ray fluorescence (XRF) on flux-fused pellets at the Hamilton College Analytical Lab (https://www.hamilton.edu/academics/analytical-lab).

Calculations in MELTS were performed isobarically at 200 MPa, which is the approximate emplacement pressure of the Duluth Complex estimated from the ~7 km overburden of the North Shore Volcanic Group (*21*). Oxygen fugacities for intrusive bodies of the Duluth Complex have been determined from the composition of co-existing Fe-Ti oxides (*31*), and indicate conditions close to the quartz-fayalite-magnetite (QFM) buffer. Therefore, our calculations in MELTS were performed using this *f* O2 constraint. Because the initial H_2O wt.% of the FC-1 parental melts is not known, multiple calculations were performed by changing the initial H_2O content. The parental magmas to the anorthositic series of the DC were nominally anhydrous (*i.e.*, H_2O wt% < 0.5) tholeiitic basalts (*21*), so H_2O contents were varied from 0.05 to 0.5 wt.%, in 0.025 wt.% increments. Calculations began by determining the liquidus temperature of the melt at each prescribed H_2O content, followed by equilibrium phase-assemblage calculations performed between this temperature and near-solidus conditions (730˚C) in 0.5 ˚C steps.

For the zircon crystallization model, the MELTS simulations were combined with the zircon saturation parametrization of (*13*). Using the liquid composition calculated by MELTS at each temperature step, the parameter M (*i.e.*, molar [Na+K+2Ca]/[Al*Si]) was used to calculate the Zr distribution coefficient between zircon and melt as

$$lnD_{Zr} = 10108/T(K) - 1.16 \cdot (M - 1) - 1.48$$

The value of lnD_{Zr} at each temperature step was used to estimate the Zr concentration necessary to achieve zircon saturation.

The concentration of Zr in the evolving liquid was calculated using the bulk-rock Zr determined by XRF (*i.e.*, 39 µg/g) as the initial melt concentration at the liquidus. At each temperature step, the concentration of Zr in the melt was calculated from the mass fraction of melt remaining and assuming that Zr behaved incompatibly in the modal phases. The liquid Zr concentration calculations proceeded in this way until the calculated melt concentration value was equal to that needed to saturate zircon. Once zircon saturation was reached, the amount of removed zircon at each step was estimated using mass balance and assuming that the melt was kept at Zr saturation during the remaining cooling path.

Results from our numerical zircon saturation calculations are in excellent agreement with petrographic observations (figs. S1, S2), which impose the constraint that zircon in FC-1 is a late-stage phase that precipitated during internal differentiation of trapped intercumulus liquids. Our combined petrographic and modeling observations are therefore in line with zircon and baddeleyite as having crystallized within a closed-system, at trapped liquid fractions that were low enough to impede chemical exchange between melt pockets and with external liquid sources (see text for discussion).

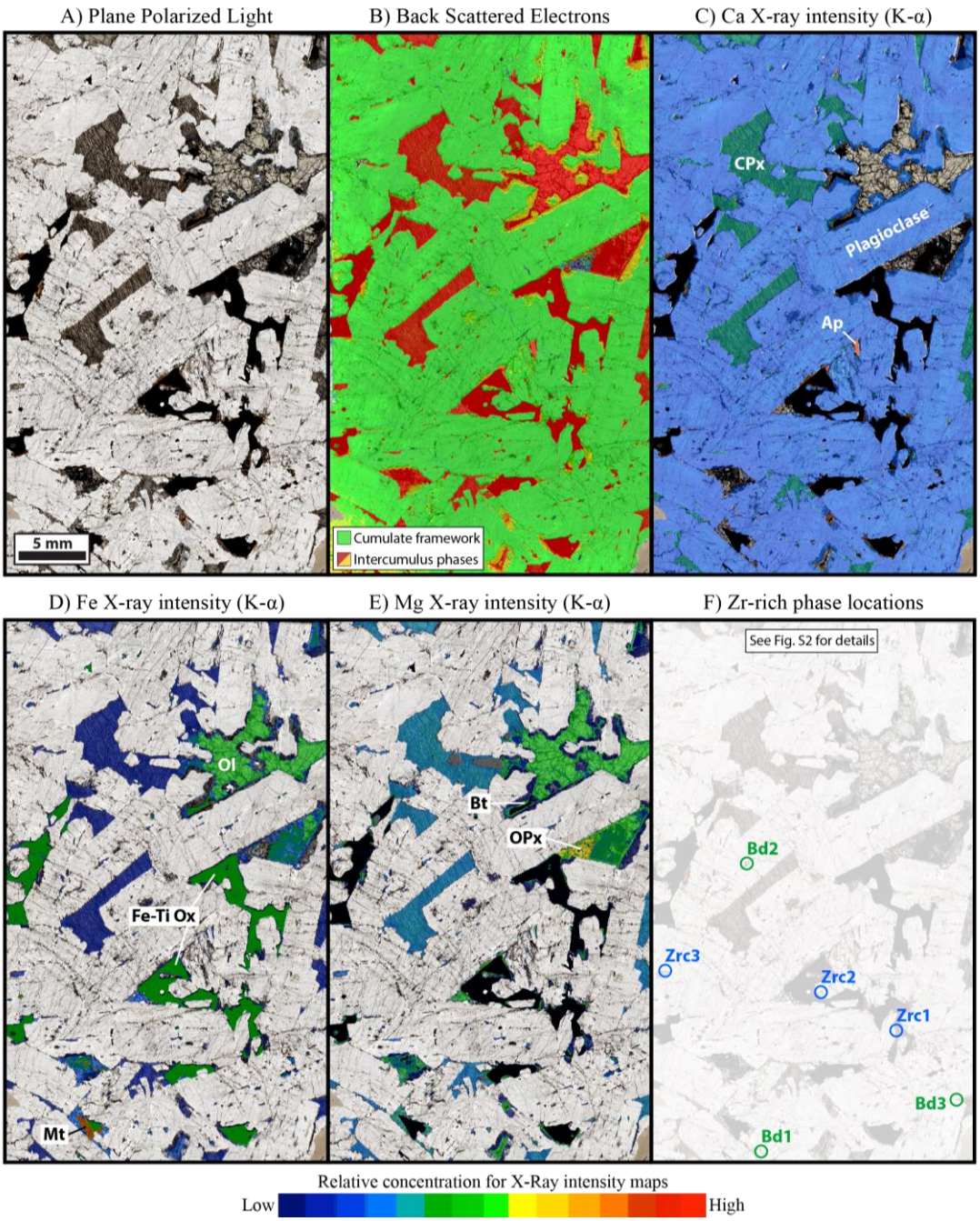

Fig. S1. Textural relations among modal phases and Zr-rich accessory phases in the FC-1 anorthositic cumulate. A) Transmitted plane-polarized light photomicrograph; B) Electron Micro-Probe (EMP) back scattered electron map; C) EMP X-Ray Ca intensity map; D) EMP X-Ray Fe intensity map; E) EMP X-Ray Mg intensity map; F) Location of Zr-rich accessory phases detailed in fig. S2. Abbreviations: Apatite (Ap); Baddeleyite (Bd); Biotite (Bt); Clinopyroxene (CPx); Fe-Ti oxides (Fe-Ti Ox); Magnetite (Mt); Olivine (Ol); Orthopyroxene (OPx); Plagioclase (Plag); Zircon (Zrc).

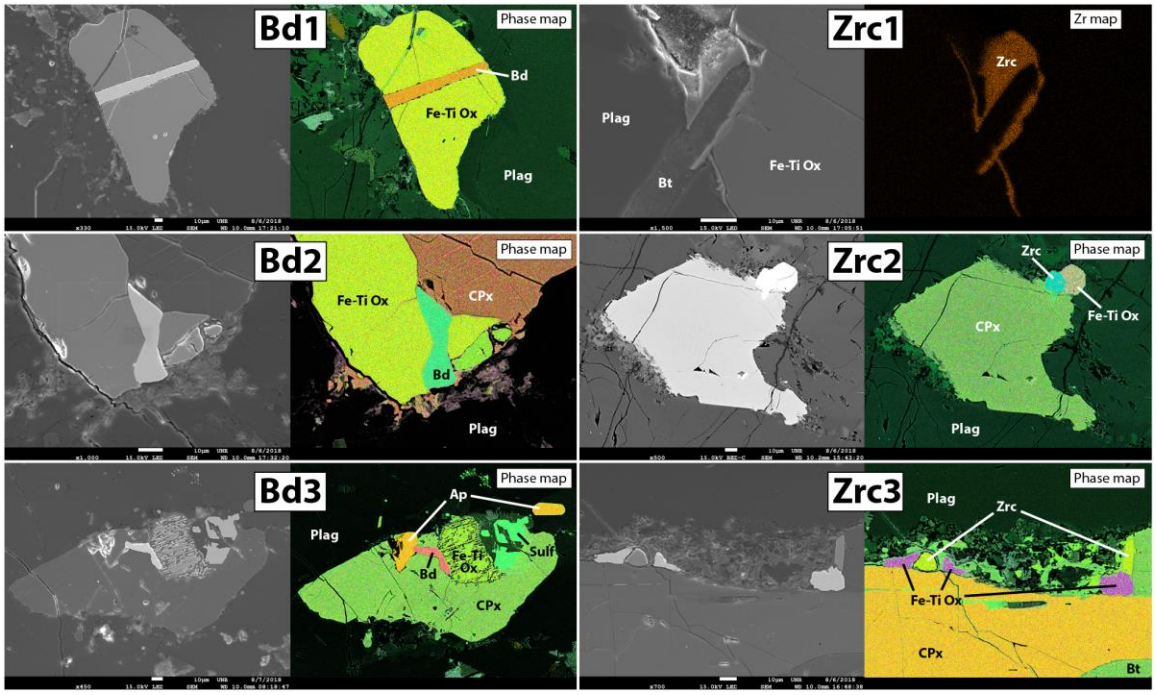

Fig. S2. Textural relations between Zr-rich accessory phases and modal phases in the FC-1 anorthositic cumulate. See fig. S1 for locations and abbreviations. For most detailed maps: left is SEM secondary electron map, right is phase map automatically constructed by the Oxford Instruments AZTEC software, based on EDS compositional maps. Only for Zrc1 the right figure is a Zr EDS compositional map, rather than a phase map.

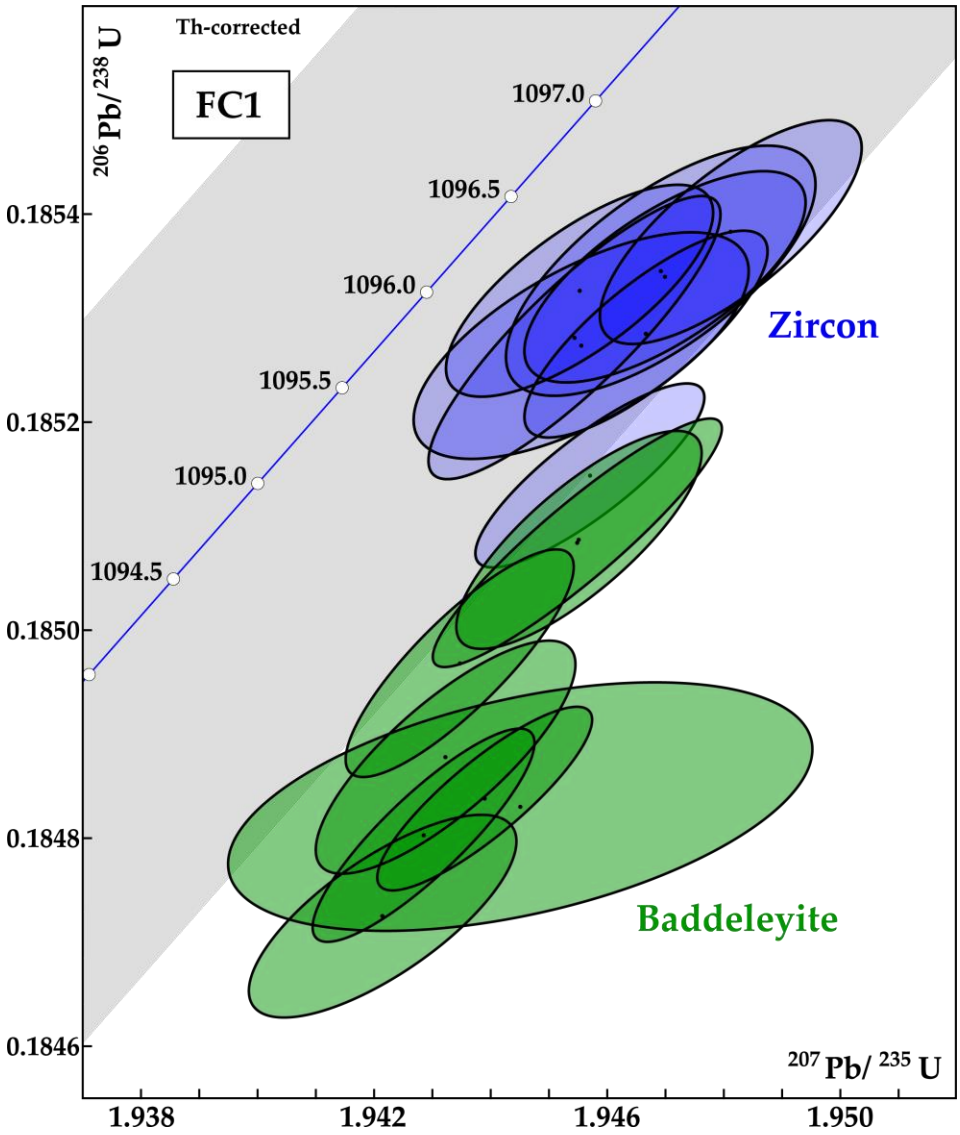

Fig. S3. U-Pb (Wetherill) concordia diagram for FC-1 zircon (blue) and baddeleyite (green) single crystals dated by (±CA)-ID-TIMS. Blue curve is the 'best-fit' concordia using the decay constants of (*47*) and the gray region reflects decay constant uncertainties.

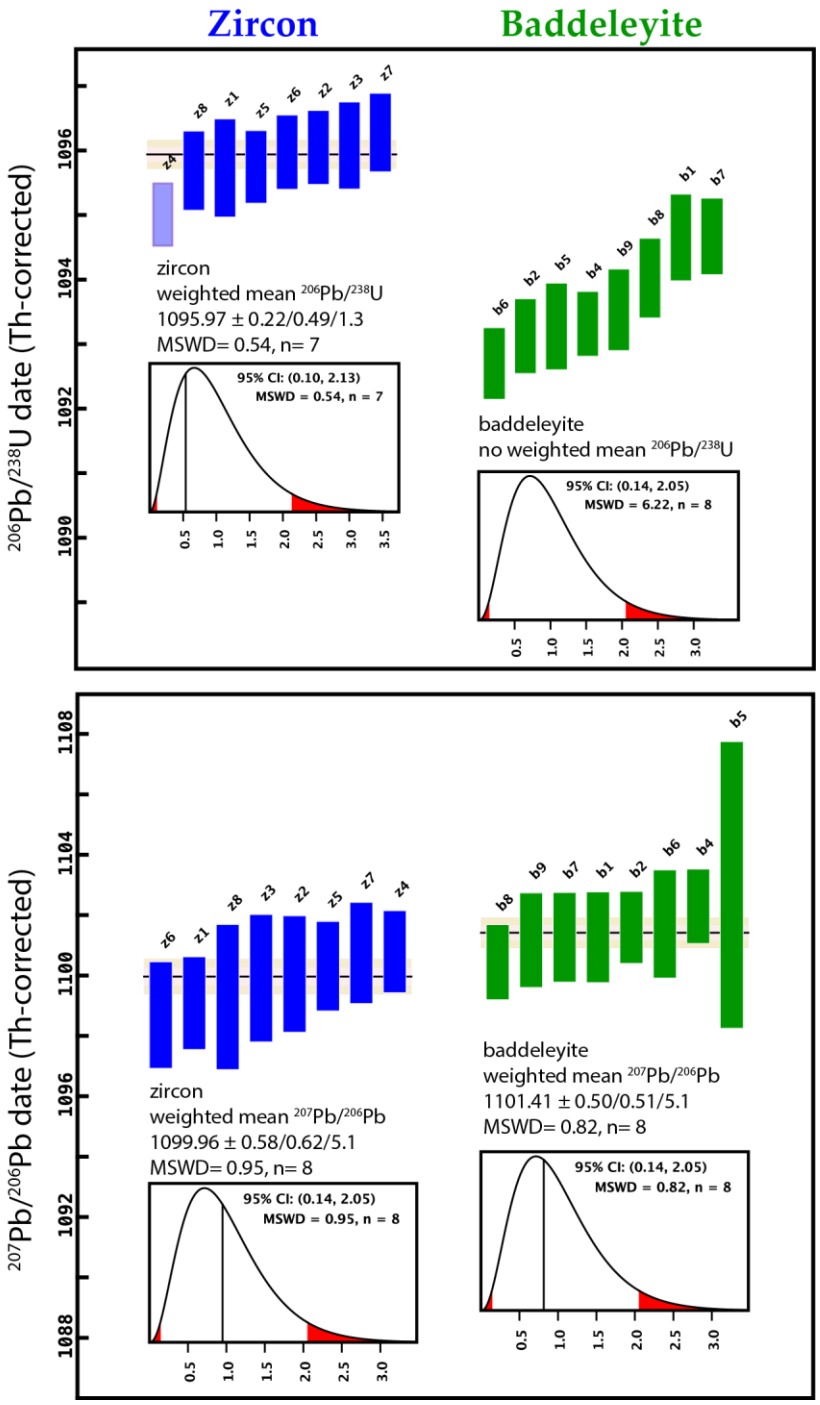

Fig. S4. Apparent ^{206}Pb/^{238}U and ^{207}Pb/^{206}Pb dates of zircon and baddeleyite single-crystals from FC-1, obtained by (±CA)-ID-TIMS. Apparent ^{206}Pb/^{238}U (top panel) and ^{207}Pb/^{206}Pb (bottom panel) dates of FC-1 zircon (red) and baddeleyite (green) crystals dated by (±CA)-ID-TIMS. Weighted mean dates are calculated for all groups of data with the exception of baddeleyite ^{206}Pb/^{238}U dates which yield an MSWD= 6.2. This large MSWD value indicates that these dates do not represent a single age population.

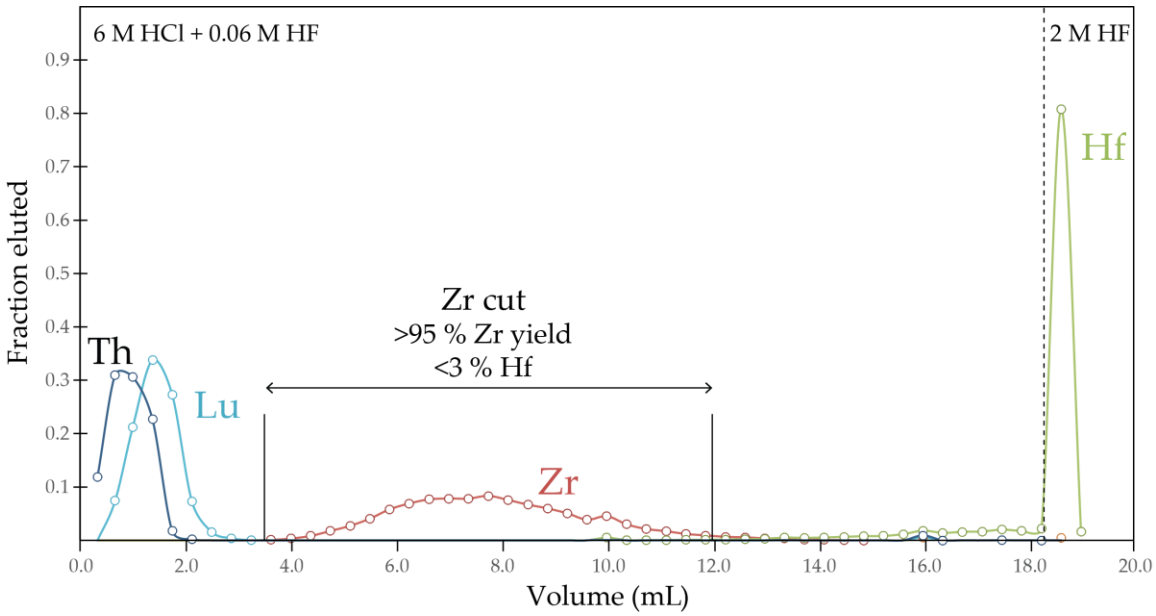

Fig. S5. Elution curve of the Ln-Spec ion-exchange chemistry optimization used to purify Zr from zircon and baddeleyite samples.

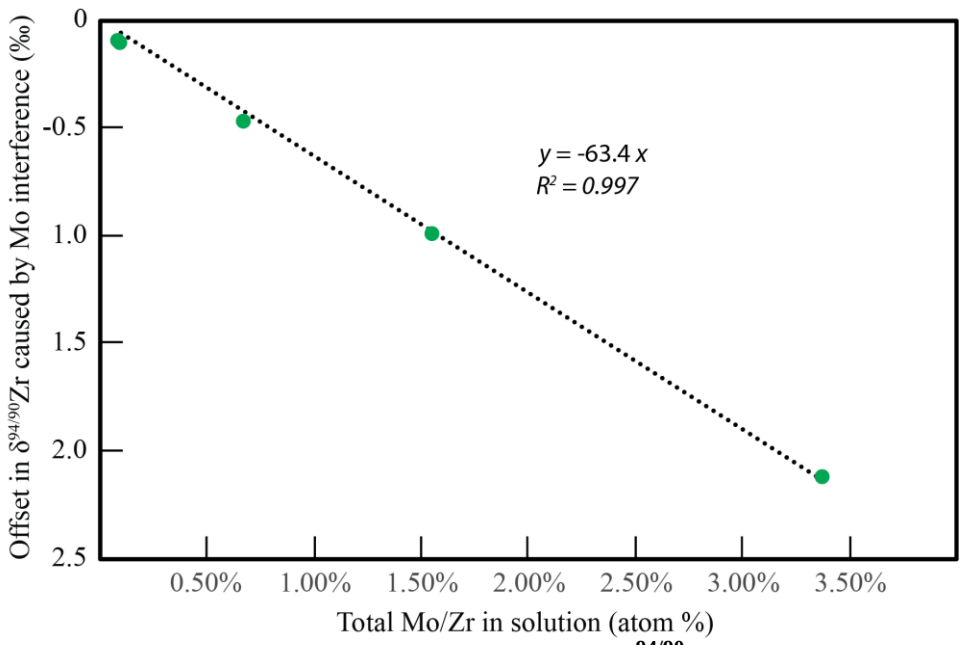

Fig. S6. Doping test performed to quantify the offsets in $\delta^{94/90}$Zr induced by residual Mo isobaric interferences.

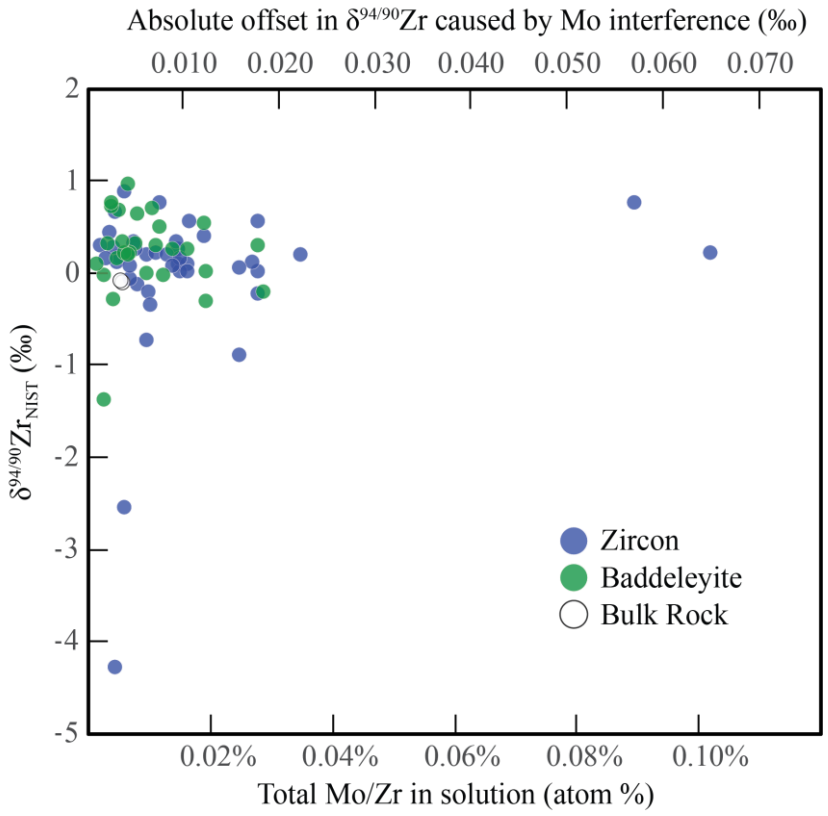

Fig. S7. $\delta^{94/90}$Zr values of zircon, baddeleyite, and bulk-rock aliquots of FC-1 gabbro as a function of residual Mo interference in the measured solutions. Bottom axis represents the total Mo/Zr atomic ratio measured in each sample. Top axis shows the absolute per mil effect of the measured Mo/Zr values on the $\delta^{94/90}$Zr composition of each fraction, calculated using the doping test results shown in fig. S6.

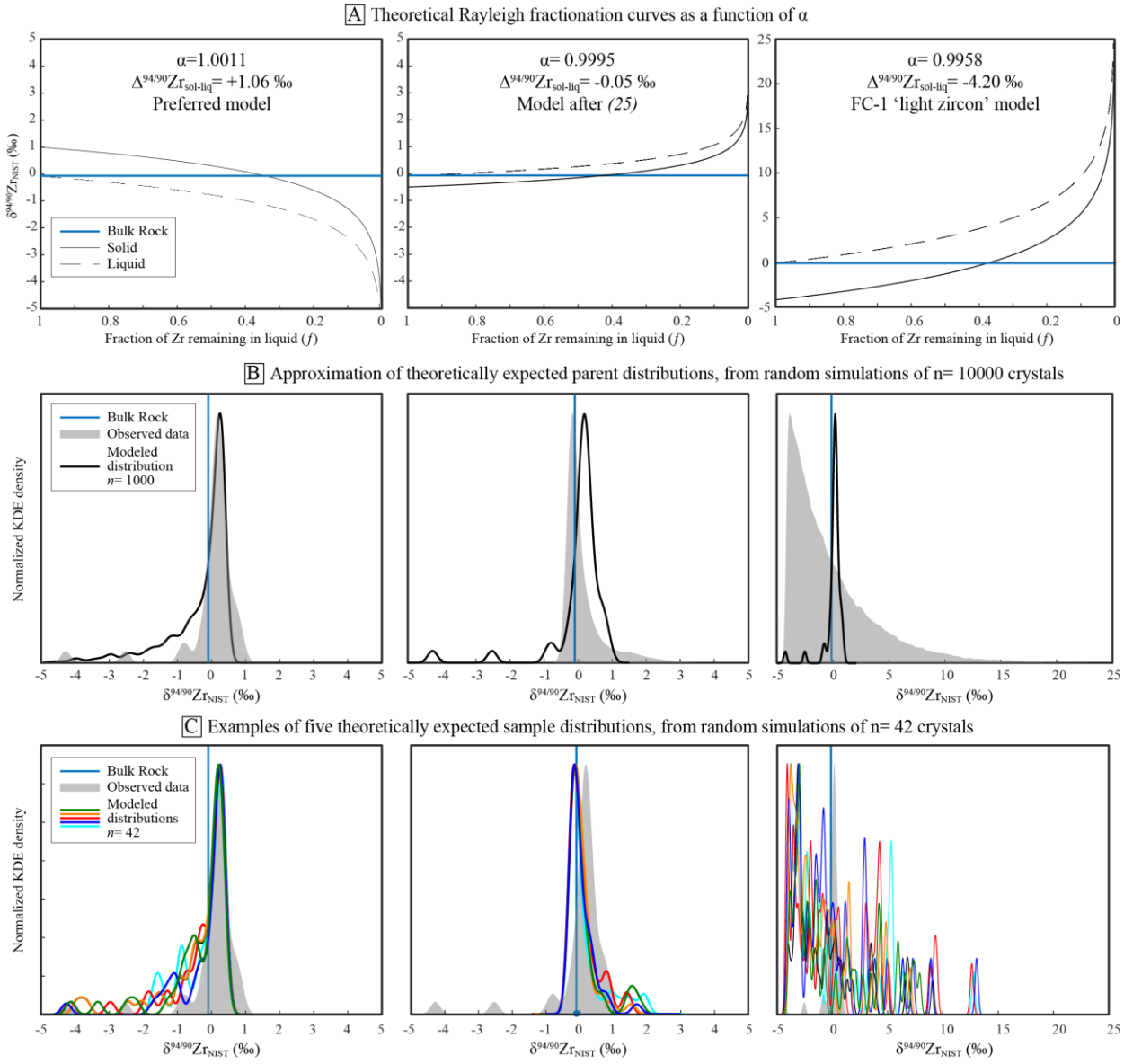

Fig. S8. Results of the Monte Carlo simulations exploring the predicted distribution of bulk zircon $\delta^{94/90}$Zr values for FC-1 as a function of different isotopic fractionation coefficients. Left column is the preferred model as discussed in the main text; central column uses the fractionation coefficient of (*23*); right column is the FC-1 'light zircon' model, calculated by assuming that zircon is isotopically light relative to co-existing melt and using the minimum magnitude of $\alpha_{sol\text{-}liq}$ that would be needed in order to explain the 'lightest' $\delta^{94/90}$Zr value observed in our dataset.

Table S1. Results of U-Pb isotopic analyses of FC-1 zircon and baddeleyite crystals using ID-TIMS (isotope dilution–thermal ionization mass spectrometry).

	Composition				Isotopic Ratios									Dates (Ma) *						
FC-1 Fraction	Pb_c (pg) *a*	Pb*/ Pb_c *b*	mass U (ng)	Th/ U *c*	$^{206}Pb/^{204}Pb$ §	$^{208}Pb/^{206}Pb$ †	$^{205}Pb/^{238}U$ †	±2σ %	$^{207}Pb/^{235}U$ †	±2σ %	Corr. coef.	$^{207}Pb/^{206}Pb$ †	±2σ %	$^{206}Pb/^{238}U$ ‡	±2σ abs	$^{207}Pb/^{235}U$ e	±2σ abs	$^{207}Pb/^{206}Pb$ e	±2σ abs	% disc *c*
zircon																				
z1	0.38	976	1.9	0.60	55875	0.180	0.18527	0.073	1.9454	0.13	0.870	0.076192	0.067	1095.76	0.74	1096.88	0.86	1099.2	1.5	0.32
z2	0.36	191	0.34	0.58	10994	0.176	0.18533	0.055	1.9470	0.12	0.702	0.076229	0.088	1096.08	0.55	1097.41	0.83	1100.2	1.9	0.38
z3	0.39	181	0.35	0.63	10279	0.189	0.18533	0.065	1.9469	0.14	0.689	0.076224	0.098	1096.11	0.65	1097.39	0.91	1100.1	2.1	0.36
z4	0.35	357	0.65	0.41	21441	0.122	0.185134	0.048	1.9457	0.10	0.847	0.076258	0.057	1095.04	0.48	1096.97	0.68	1100.9	1.3	0.54
z5	0.36	350	0.67	0.37	21191	0.111	0.185270	0.054	1.9467	0.11	0.801	0.076240	0.064	1095.78	0.54	1097.30	0.72	1100.5	1.4	0.43
z6	0.45	214	0.48	0.56	12368	0.168	0.18531	0.055	1.9455	0.12	0.736	0.076177	0.080	1096.01	0.55	1096.91	0.79	1098.8	1.7	0.26
z7	0.35	252	0.46	0.38	15280	0.113	0.18537	0.058	1.9481	0.12	0.751	0.076256	0.075	1096.31	0.59	1097.80	0.77	1100.9	1.6	0.42
z8	0.34	146	0.24	0.64	8264	0.192	0.18526	0.059	1.9456	0.15	0.657	0.076200	0.11	1095.72	0.59	1096.91	0.99	1099.4	2.4	0.34
baddeleyite																				
b1	0.52	455	1.4	0.009	30334	0.00284	0.18507	0.065	1.9455	0.13	0.919	0.076277	0.065	1094.69	0.65	1096.89	0.85	1101.4	1.5	0.62
b2	0.54	544	1.7	0.014	36235	0.00436	0.18479	0.055	1.9428	0.098	0.865	0.076289	0.047	1093.16	0.56	1095.98	0.66	1101.8	1.1	0.79
b4	0.50	459	1.3	0.011	30622	0.00321	0.184821	0.048	1.9439	0.095	0.858	0.076316	0.050	1093.35	0.48	1096.34	0.64	1102.5	1.2	0.84
b5	1.88	50	0.55	0.016	3343	0.00478	0.18481	0.065	1.9445	0.26	0.461	0.07634	0.23	1093.31	0.65	1096.6	1.7	1103.2	4.7	0.90
b6	1.41	170	1.4	0.007	11338	0.00212	0.184708	0.053	1.9421	0.12	0.738	0.076294	0.081	1092.74	0.53	1095.74	0.79	1101.9	1.7	0.84
b7	0.35	281	0.57	0.015	18734	0.00451	0.18507	0.057	1.9455	0.11	0.796	0.076277	0.064	1094.70	0.57	1096.90	0.73	1101.4	1.4	0.62
b8	0.47	685	1.9	0.017	45582	0.00499	0.18495	0.059	1.9435	0.10	0.846	0.076245	0.050	1094.06	0.60	1096.20	0.68	1100.6	1.2	0.60
b9	1.05	233	1.4	0.023	15522	0.00682	0.18486	0.061	1.9432	0.11	0.796	0.076273	0.069	1093.57	0.61	1096.11	0.77	1101.4	1.5	0.71

a Total mass of common Pb.

b Ratio of radiogenic Pb (including ^{208}Pb) to common Pb.

c Th contents calculated from radiogenic ^{208}Pb and ^{230}Th-corrected $^{206}Pb/^{238}U$ date of the sample, assuming concordance between U-Pb Th-Pb systems.

§ Measured ratio corrected for fractionation and spike contribution only.

† Measured ratios corrected for fractionation (α = 0.18 ± 0.02 %/amu), tracer (ET-535; Condon et al., 2015), and the MIT laboratory blank composition.

‡ Corrected for initial Th/U disequilibrium using radiogenic ^{208}Pb and Th/U[magma] = 2.8.

* Isotopic dates calculated using λ238 = 1.55125E-10 (Jaffey et al. 1971) and λ235 = 9.8485E-10 (Jaffey et al. 1971).

% discordance = 100 - (100 * ($^{206}Pb/^{238}U$ date) / ($^{207}Pb/^{206}Pb$ date))

Table S2. Assignment of *f* values for zircon and baddeleyite from FC-1, and uncertainty limits imposed by different magnitudes of fractional growth integration history according to Fig. 3.

			Fractional integ. = 0.2		Fractional integ. = 0.4		Fractional integ. = 0.6		Fractional integ. = 0.8		Fractional integ. = 0.95	
zircon*	$\delta^{94/90}$Zr	*f* instant	Max. initial *f*	Min. final *f*	Max. initial *f*	Min. final *f*	Max. initial *f*	Min. final *f*	Max. initial *f*	Min. final *f*	Max. initial *f*	Min. final *f*
3_z11	+0.905	0.06	0.00	0.12	0.00	0.12	0.00	0.12	0.00	0.12	0.00	0.12
z8	+0.776	0.17	0.07	0.26	0.00	0.33	0.00	0.33	0.00	0.33	0.00	0.33
3_z2	+0.770	0.17	0.08	0.26	0.00	0.34	0.00	0.34	0.00	0.34	0.00	0.34
3_z1	+0.679	0.24	0.16	0.32	0.04	0.42	0.00	0.46	0.00	0.46	0.00	0.46
z6	+0.583	0.31	0.23	0.38	0.13	0.47	0.00	0.57	0.00	0.57	0.00	0.57
z13	+0.581	0.31	0.23	0.38	0.13	0.48	0.00	0.58	0.00	0.58	0.00	0.58
3_z9	+0.450	0.39	0.32	0.46	0.23	0.54	0.10	0.64	0.00	0.71	0.00	0.71
z11	+0.420	0.41	0.34	0.47	0.25	0.55	0.12	0.65	0.00	0.74	0.00	0.74
3_z8	+0.362	0.44	0.37	0.50	0.29	0.57	0.17	0.67	0.00	0.78	0.00	0.78
4_z1R	+0.348	0.45	0.38	0.51	0.30	0.58	0.18	0.67	0.00	0.79	0.00	0.79
3_z13	+0.336	0.45	0.39	0.51	0.31	0.58	0.19	0.68	0.00	0.80	0.00	0.80
3_z16	+0.315	0.46	0.40	0.52	0.32	0.59	0.21	0.68	0.02	0.80	0.00	0.82
3_z5	+0.301	0.47	0.41	0.53	0.33	0.60	0.22	0.69	0.04	0.81	0.00	0.83
3_z6	+0.278	0.48	0.42	0.54	0.34	0.61	0.23	0.69	0.06	0.81	0.00	0.84
z10	+0.266	0.49	0.43	0.54	0.35	0.61	0.24	0.70	0.07	0.81	0.00	0.85
4_z2R	+0.227	0.51	0.45	0.56	0.37	0.62	0.27	0.71	0.10	0.82	0.00	0.88
z2	+0.222	0.51	0.45	0.56	0.38	0.63	0.27	0.71	0.10	0.82	0.00	0.88
z4	+0.215	0.51	0.46	0.56	0.38	0.63	0.28	0.71	0.11	0.82	0.00	0.88
4_z12R	+0.210	0.51	0.46	0.57	0.39	0.63	0.28	0.71	0.12	0.82	0.00	0.89
z16	+0.203	0.52	0.46	0.57	0.39	0.63	0.29	0.71	0.12	0.82	0.00	0.89
3_z3	+0.197	0.52	0.46	0.57	0.39	0.64	0.29	0.72	0.13	0.82	0.00	0.89
3_z17	+0.174	0.53	0.48	0.58	0.41	0.64	0.31	0.72	0.14	0.83	0.00	0.91
4_z13R	+0.174	0.53	0.48	0.58	0.41	0.64	0.31	0.72	0.14	0.83	0.00	0.91
4_z5R	+0.131	0.55	0.50	0.60	0.43	0.66	0.33	0.73	0.18	0.84	0.00	0.93
3_z10	+0.125	0.55	0.50	0.60	0.43	0.66	0.34	0.73	0.18	0.84	0.00	0.93
z5	+0.117	0.55	0.50	0.60	0.44	0.66	0.34	0.74	0.19	0.84	0.00	0.93
z7	+0.113	0.56	0.51	0.60	0.44	0.66	0.34	0.74	0.19	0.84	0.00	0.94
3_z14	+0.098	0.56	0.51	0.61	0.45	0.67	0.35	0.74	0.20	0.84	0.00	0.94
4_z17R	+0.092	0.56	0.52	0.61	0.45	0.67	0.36	0.74	0.21	0.84	0.00	0.95
4_z6R	+0.065	0.58	0.53	0.62	0.46	0.68	0.37	0.75	0.23	0.85	0.01	0.95
4_z7R	+0.034	0.59	0.54	0.63	0.48	0.69	0.39	0.76	0.25	0.85	0.04	0.95
4_z9R	+0.024	0.59	0.55	0.64	0.48	0.69	0.40	0.76	0.26	0.85	0.05	0.95
z12	+0.021	0.59	0.55	0.64	0.49	0.69	0.40	0.76	0.26	0.85	0.05	0.95
3_z4	-0.046	0.62	0.57	0.66	0.52	0.71	0.44	0.77	0.31	0.86	0.11	0.96
z14	-0.106	0.64	0.60	0.68	0.54	0.73	0.47	0.79	0.34	0.87	0.16	0.96
3_z15	-0.197	0.67	0.63	0.70	0.58	0.75	0.51	0.80	0.40	0.88	0.23	0.96
4_z10R	-0.220	0.68	0.64	0.71	0.59	0.75	0.52	0.81	0.41	0.88	0.25	0.96
4_z15R	-0.333	0.71	0.68	0.74	0.63	0.78	0.57	0.83	0.47	0.89	0.32	0.97
z1	-0.714	0.80	0.77	0.82	0.74	0.85	0.70	0.88	0.63	0.93	0.53	0.98
z3	-0.883	0.83	0.81	0.85	0.78	0.87	0.74	0.90	0.69	0.94	0.60	0.98
3_z7	-2.530	0.96	0.96	0.97	0.95	0.97	0.95	0.98	0.93	0.99	0.92	1.00
3_z12	-4.278	0.99	0.99	0.99	0.99	0.99	0.99	1.00	0.99	1.00	0.98	1.00
baddeleyite												
3_b8*	+0.971	0.00	0.00	0.00	0.00	0.00	0.00	0.00	0.00	0.00	0.00	0.00
3_b10	+0.773	0.17	0.08	0.26	0.00	0.33	0.00	0.33	0.00	0.33	0.00	0.33
3_b7	+0.740	0.20	0.11	0.28	0.00	0.38	0.00	0.38	0.00	0.38	0.00	0.38
b6	+0.719	0.21	0.12	0.30	0.00	0.40	0.00	0.41	0.00	0.41	0.00	0.41
b4	+0.692	0.23	0.14	0.32	0.03	0.42	0.00	0.44	0.00	0.44	0.00	0.44
3_b13	+0.656	0.26	0.17	0.34	0.06	0.44	0.00	0.49	0.00	0.49	0.00	0.49
b3	+0.554	0.33	0.25	0.40	0.15	0.49	0.01	0.60	0.00	0.61	0.00	0.61
b11	+0.522	0.35	0.27	0.42	0.17	0.50	0.03	0.61	0.00	0.64	0.00	0.64
3_b6	+0.344	0.45	0.38	0.51	0.30	0.58	0.18	0.67	0.00	0.80	0.00	0.80
b1	+0.333	0.45	0.39	0.51	0.31	0.59	0.19	0.68	0.01	0.80	0.00	0.80
b9	+0.329	0.46	0.39	0.51	0.31	0.59	0.20	0.68	0.01	0.80	0.00	0.81
4_b3	+0.311	0.46	0.40	0.52	0.32	0.59	0.21	0.68	0.03	0.80	0.00	0.82
b5	+0.308	0.47	0.41	0.52	0.33	0.59	0.21	0.68	0.03	0.81	0.00	0.82
b2	+0.270	0.48	0.43	0.54	0.35	0.61	0.24	0.70	0.06	0.81	0.00	0.85
4_b2	+0.266	0.49	0.43	0.54	0.35	0.61	0.24	0.70	0.07	0.81	0.00	0.85
3_b5	+0.241	0.50	0.44	0.55	0.37	0.62	0.26	0.70	0.09	0.82	0.00	0.87
b12	+0.223	0.51	0.45	0.56	0.38	0.63	0.27	0.71	0.10	0.82	0.00	0.88
3_b9	+0.212	0.51	0.46	0.57	0.38	0.63	0.28	0.71	0.11	0.82	0.00	0.88
3_b4	+0.180	0.53	0.47	0.58	0.40	0.64	0.30	0.72	0.14	0.83	0.00	0.90
3_b14	+0.115	0.55	0.50	0.60	0.44	0.66	0.34	0.74	0.19	0.84	0.00	0.93
b7	+0.023	0.59	0.55	0.64	0.48	0.69	0.40	0.76	0.26	0.85	0.05	0.95
b8	+0.007	0.60	0.55	0.64	0.49	0.70	0.41	0.76	0.27	0.85	0.07	0.95
b10	-0.009	0.60	0.56	0.65	0.50	0.70	0.42	0.77	0.28	0.86	0.08	0.95
3_b12	-0.011	0.60	0.56	0.65	0.50	0.70	0.42	0.77	0.28	0.86	0.08	0.95
4_b1	-0.192	0.67	0.63	0.70	0.58	0.75	0.51	0.80	0.40	0.88	0.23	0.96
3_b3	-0.277	0.69	0.66	0.73	0.61	0.77	0.55	0.82	0.44	0.89	0.29	0.96
4_b5	-0.286	0.70	0.66	0.73	0.62	0.77	0.55	0.82	0.45	0.89	0.29	0.96
3_b2	-1.359	0.89	0.88	0.90	0.86	0.92	0.84	0.93	0.80	0.96	0.74	0.99

* Rank ordered from most positive to most negative $\delta^{94/90}$Zr value.